Kinetics of Temperature Response of PEO-b-PNIPAM-b-PAA Triblock Terpolymer Aggregates and of their Complexes with Lysozyme

Aristeidis Papagiannopoulos[1,*], Anastasia Meristoudi[1], Kunlun Hong[2] and Stergios Pispas[1,*]

[1]Theoretical and Physical Chemistry Institute, National Hellenic Research Foundation, 11635 Athens, Greece

[2]Center for Nanophase Materials Sciences, Oak Ridge National Laboratory, 2008 Oak Ridge TN, USA

* E-mail address of presenting author: apapagiannopoulos@eie.gr

ABSTRACT

The doubly stimuli responsive triblock terpolymer PEO-b-PNIPAM-b-PAA and its interaction with lysozyme is studied by Multi Angle Laser Light Scattering. The kinetics of the response during temperature jumps crossing the PNIPAM lower critical transition temperature (LCST) of the pure polymer and polymer/protein complexes; and the kinetics of protein complexation with the polymer at room temperature are analysed. By monitoring the apparent molecular weight, the radius of gyration and hydrodynamic radius, we can characterize the shape and mass of the formed aggregates. We find that the coil-to-globule transition of PNIPAM creates new bonds within the aggregates that are irreversible when the temperature is decreased below the lower critical transition temperature (LCST) of the transition. Additionally the internal dynamics of PnBA-b-PNIPAM-b-PAA aggregates and PnBA-b-PNIPAM-b-PAA / lysozyme complexes are “frozen” irreversibly when the temperature is raised above the LCST.

INTRODUCTION

Macromolecular compounds self-assembled in aqueous solutions, produce nano-scale formulations that are candidates for carriers in targeted drug and protein delivery, bio-sensors, and tissue engineering[1]. The choice of the monomeric units can be made so that the resulting polymers respond to external stimuli, such as pH and salt concentration (for charged polymers) and temperature (for thermoresponsive polymers). Nanoparticles with hydrophobic cores, and coronas made of water-soluble (neutral micelles) or charged macromolecular chains (polyelectrolyte micelles) provide a template for drug loading either on the hydrophobic core via hydrophobic interactions[2] (in both cases) or via electrostatic attraction[3] with the corona (in the case of polyelectrolyte micelles). Charged or neutral nanogels[4] made of physically or chemically cross-linked macromolecules and polymeric aggregates[5] may also be utilized as pharmaceutical carriers. The kinetics of the response of a nanoscopic system to an external stimulus is of practical importance for its applications and its study reveals inherent information on its morphological transitions towards equilibrium under the changed conditions.

PNIPAM-containing macromolecules have been extensively studied and used in biomedical applications[6, 7] since PNIPAM exhibits a lower critical solution temperature (LCST) at about 32 ºC, which is near the physiological temperature. PAA is a weak polyacid that is a common pH-sensitive polyelectrolyte (with a pK_a=4.2) and PEO is a well-known water soluble, non-ionic, biocompatible polymer. Combination of these three blocks in one triblock terpolymer chain is expected to provide a rich content of stimuli responsive properties to a water soluble biocompatible polymeric compound.

In this work we use Multi-Angle Laser Light Scattering to study the kinetics of: 1) the temperature response of PEO-b-PNIPAM-b-PAA with temperature jumps from below to above the LCST of PNIPAM and vice-versa, 2) the complexation between PEO-b-PNIPAM-b-PAA with the model globular protein lysozyme and 3) the temperature response of the formed triblock terpolymer/protein complexes during temperature jumps. The feature of multi-detection at many angles simultaneously allows us to obtain the morphological parameters of the nano-structures and follow the kinetics of the ongoing processes.

EXPERIMENTAL METHODS

The tri-block terpolymer, poly(ethylene oxide)-block-poly(N-isopropylacrylamide)-block-poly(acrylic acid) (PEO-b-PNIPAM-b-PAA) was synthesized using reversible addition-fragmentation chain transfer (RAFT) polymerization. The resulting M_w is $M=56\cdot10^3$ g/mol and the respective weight contents are 7% for PEO, 68% for PNIPAM and 25% for PAA. The polymer was dissolved in water (pH 7) at 0.1 mg/ml. The sample was left overnight to equilibrate and the salt content was set afterwards to 0.01M NaCl.

Lysozyme (HEWL) with molecular weight $M=14.7\cdot10^3$ g/mol was purchased from Fluka and used without further purification. Stock solutions were prepared by dissolving lysozyme at 0.1 mg/ml in the pH7/0.01M NaCl aqueous medium and leaving overnight to equilibrate. All samples were filtered by 0.45μm hydrophilic sartorious filters in order to eliminate dust or large clusters and loaded into standard 1cm width Helma quartz dust - free cells.

Multi Angle Laser Light Scattering was performed with an ALV compact goniometer system (ALVGmbH, Germany), equipped with four ALV-5000/EPP multi tau digital correlators and a He-Ne laser operating at the wavelength of 632.8 nm able to perform

a full static and dynamic measurement at 16 angles (from 20 to 146°) in 7 minutes. In Static Light Scattering (SLS) the Rayleigh ratio $R(q)$ is calculated with respect to a toluene standard. The scattering wave vector is given by $q = \frac{4\pi n_0}{\lambda} sin\frac{\theta}{2}$ where n_0 is the solvent's refractive index.

SLS data were treated[8] by the Zimm approximation:

$$\frac{Kc}{R(q,c)} = \frac{1}{M_w P(q)} \qquad (1)$$

M_w is the z-averaged molar mass and c is the particle mass-concentration in solution. In case of an aggregating polymer of molecular weight M_{pol} in solution the aggregation number (N_{agg}) is given by $N_{agg} = \frac{M_w}{M_{pol}}$. The single particle's form factor is given by $P(q) = \left(1 + \frac{1}{3}q^2 R_g^2\right)^{-1}$ (Zimm) or $P(q) = e^{-\frac{1}{3}q^2 R_g^2}$(Guinier approximation), where R_g the (z-averaged) radius of gyration. K is the contrast factor for LS given by $K = \frac{4\pi^2 n_0^2}{N_A \lambda^4}(\partial n/\partial c)^2$, where $\partial n/\partial c$ is the refractive index increment of the scattering particles in the solvent.

In Dynamic Light Scattering (DLS) the intensity auto-correlation functions $g^{(2)}(t)$ are collected[9] at different scattering angles and can be analysed by the CONTIN algorithm. The characteristic relaxation rate $\Gamma(q)$ is taken from the position of the maximum ($\tau(q)$) of the distribution function of relaxation times ($\Gamma(q) = \frac{1}{\tau(q)}$). In the case of diffusive modes there is a linear relation between $\Gamma(q)$ and q^2 i.e. $\Gamma(q) = D \cdot q^2$ and hence the diffusion coefficient D is obtained. The hydrodynamic radius, R_h, is extracted from the Stokes-Einstein equation (equation 2).

$$R_h = \frac{k_B T}{6\pi\eta D} \qquad (2)$$

where η is the viscosity of the solvent, k_B is the Boltzmann constant and T is the absolute temperature. The temperature of the samples was set by a PolyScience

temperature controller. For an increasing-temperature jump the sample cell was removed from the sample holder, the sample holder/toluene bath was heated to the desired temperature and the sample was rapidly inserted into the sample environment. All the samples were tested at 25 and 30 °C before any increasing-temperature jump and no morphology change was observed. For the decreasing-temperature jumps the desired temperature was set in the bath without removing the sample and going on with the data collection. The temperature inside the sample-containing toluene bath did not take longer than 5 minutes to reach the set point.

RESULTS AND DISCUSSION

Kinetics of PEO-b-PNIPAM-b-PAA assembly. In figure 1a the SLS data from a 30 to 35 °C temperature jump is shown for several instants after the temperature jump. The data are presented as Guinier plots. It is clear that the intercept is increasing as a function of time indicating the increase in molecular weight. The initial slope is also changing which highlights the change in the radius of gyration. The low-q range of our LS measurements (3-4 first data points) allows determination of R_g values up to ~200-250 nm. As it can be shown[10] the Guinier approximation estimates R_g with 10% accuracy up to $qR_g \approx 2$. In this work we use the initial linear part of the Guinier plots to estimate R_g and M_w. The divergence of Guinier plots from linearity at higher q can be attributed to either effects of the form factor of the scattering objects[11] or co-presence of species of smaller R_g in solution.

In DLS the intensity auto-correlation functions were characterized by a single mode (CONTIN peak) and from them the characteristic relaxation rate ($\Gamma(q)$) was obtained (figure 1b). More on the CONTIN analysis distributions will be presented towards the end of the manuscript. The linear initial part of the $\Gamma(q)$ vs q^2 plots was used to

extract the diffusion coefficient and subsequently R_h. The divergence of these plots from linearity at higher q can be attributed to either internal dynamics of the scattering objects[12] or co-presence of species with higher diffusion coefficient. The analysis of the data is similar for the rest of the study in terms of measurement of R_g, R_h and M_w.

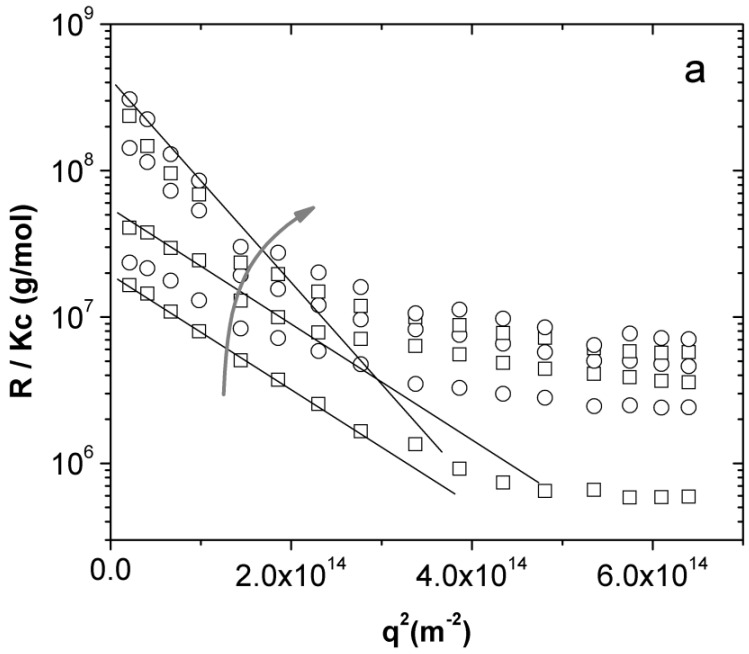

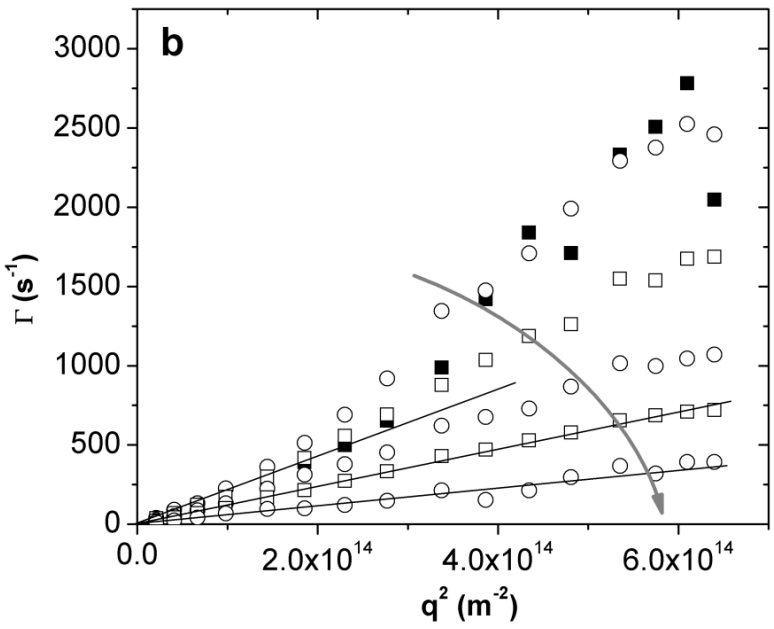

Figure 1: SLS (a) and DLS (b) data from a 30 to 35 °C temperature jump for PEO-b-PNIPAM-b-PAA (0.1mg/ml, pH 7 and 0.01M NaCl) from successive measurements about 25 min apart from each other. The bended arrows represent the passing of time. The straight lines are fits at the initial linear part of the data sets. The filled squares represent the data at the start of the experiment (hence they do not follow the time-arrow).

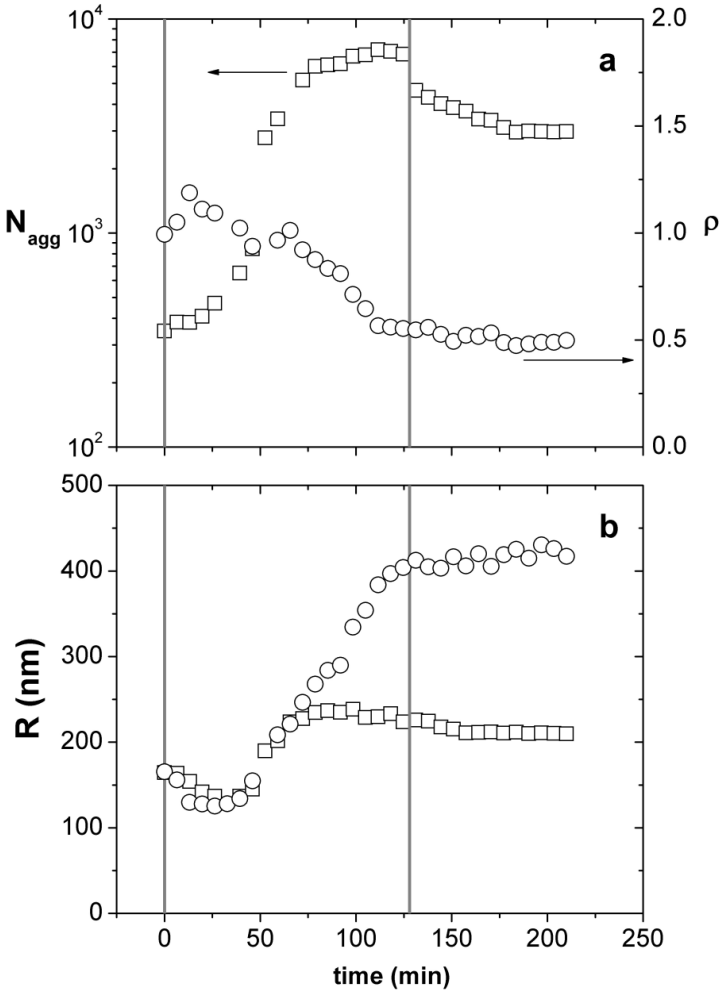

Figure 2: Aggregation number (squares) and characteristic ratio $\rho = \frac{R_g}{R_h}$ (circles) (a), and gyration (squares) and hydrodynamic radius (circles) (b), for PEO-b-PNIPAM-b-

PAA (0.1mg/ml, pH 7 and 0.01M NaCl). The vertical lines indicate the jump from 30 to 35 °C (left) and from 35 to 30 °C (right).

The apparent aggregation number N_{agg} is found much higher than unity already from 30 °C (the data was unchanged between 25 to 30 °C). Indeed in aqueous solutions, the expected unperturbed dimensions of PEO[13] ($R_g \approx 3nm$), PNIPAM[14] ($R_g \approx 8nm$, below LCST) and PAA[15] ($L \approx 50\,nm$, fully stretched) chains of similar molecular weights are small compared to the apparent sizes observed by LS. This means that the system is in an aggregated state possibly due to hydrophobic attraction between PNIPAM blocks below LCST[16, 17]. Also hydrogen bonding between PEO and PAA[18, 19] blocks is a possible cause of inter-chain associations. In the first 25 minutes after the increase-temperature jump there is a mild increase in N_{agg} and a simultaneous decrease in the radii (figure 2). The shrinkage of the aggregates is caused by the coil-to-globule transition of PNIPAM blocks[20]. We have to keep in mind that under constant N_{agg} any change in R_h in the order of 50 nm is due to a collective change in conformation of individual PNIPAM chains from the whole mass of the aggregate (because of the small size of individual PNIPAM chains). The mild increase of N_{agg} signifies the enhanced presence of hydrophobic units in the aggrregates that facilitates further aggregation although at this stage this is not the dominant effect. In the recent works of Papadaki's et al. the thermoresponsive kinetic studies of PS-b-PnNIPAM-b-PS flower-like micelles reveal an initial stage of intermicellar morphological rearrangement (collapse of the PNIPAM shell) and a subsequent intermicellar clustering[21, 22]. In that case though, the initial inter-micellar rearrangement is much faster (~10-20 sec) than ours (~20 minutes). This shows that our system, which contains two hydrophilic side blocks (e.g. PEO and PAA) instead of highly

hydrophobic ones (i.e. PS), resists to a fast internal collapse since the hydrophilic groups stabilize its structure in water.

During the initial stage (0 to 25 min) the ratio $\rho = \frac{R_g}{R_h}$ increases from $\rho \approx 1$ to $\rho \approx 1.2$. This is compatible with a geometry of a randomly cross-linked microgel [23] or a dense fractal aggregate [24]. Between 50 and 100 minutes there is a strong increase in N_{agg} due to strong clustering between aggregates. We have observed by small angle neutron scattering a similar effect of clustering of intermicellar aggregates of PS-b-PNIPAM-b-PS micelles [17] upon increasing temperature above PNIPAM's LCST. Additionally in that work, we had observed the shrinkage of the (intermicellar) aggregates as we did here.

This increase in N_{agg} is accompanied by a simultaneous strong increase in R_h. On the other hand R_g reaches a plateau value at 75 minutes and consequently from that time ρ drops below 1 eventualy reaching a value between 0.5 and 0.6. This value of ρ is reminescent of spherical particles with their mass distribution concentrated preferably towards their center [25] (dense core-diffuse shell geometry). We had observed a super-core-shell spherical geometry[17] of flower-like PS-b-PNIPAM-b-PS micelles within aggregates caused by the presence of PNIPAM. In that case a dense core of closely packed micelles was formed surrounded by loosely attached micelles. Since after 75 minutes R_g is constant while R_h increases we conclude that at this time regime aggregates adhere loosely on pre-formed denser aggregates and at the same time the initial core of the clusters collapses further. Values of ρ below the one of a uniform sphere[26] (~0.775) can be observed also for microgels[27] and there also exist observations where a dense core can further collapse while the outer periphery remains virtually unchanged, leading to a decrease in R_g while R_h remains constant[23].

After switching the temperature from 35 back to 30°C (figure 2) there is a weak drop in N_{agg} which reaches a plateau value much higher than the starting one i.e. the system does not return to its original state (the one before the temperature-increase jump) within the time-frame of the experiment. Apparently the PAA-PEO and PAA-PAA aggregations that were formed at 35 °C play a critical role. Although PNIPAM is below its LCST and its hydrophobicity is diminished at 30°C, the PEO–PAA interactions acting when these come closer within the clusters, persist after the decrease in temperature below LCST. PAA is an intrinsically hydrophobic polyelectrolyte. It has been observed that it can form collapsed layers in the case of core-shell polyelectrolyte micelles with a hydrophobic core[15]. At this situation the counterions are forced to condensate back onto the PAA backbone. This way, contacts may remain after the globule-to-coil transition of PNIPAM.

Additionally there is a weak decrease in R_g and a weak increase in R_h (at the jump from 35 back to 30°C). The increase in R_h and dissociation (to some extent) of the clusters (decrease in N_{agg}) show a relaxed conformation of the clusters below the LCST. This small increase in R_h is most probably due to the extension of PNIPAM blocks and the resulting swelling and hydration of the clusters[28]. PNIPAM blocks are hydrophilic at this temperature. The slight decrease in R_g during the dissociation of clusters can be explained by a detachment of aggregates from the outer layers of the super-core-shell structure formed at 35 ^{o}C (ρ remains near 0.5).

Kinetics of complexation and temperature response of PEO-b-PNIPAM-b-PAA / lysozyme complexes. We now turn to the PEO-b-PNIPAM-b-PAA / lysozyme nanosystems. Mixing the two components results in complexation due to the complementarity between the negative charges of PAA block and the positive ones of lysozyme. For the complexed amount of lysozyme per PEO-b-PNIPAM-b-PAA

aggregate the following procedure is used[29]. Assuming that the scattered light from free lysozyme in solution is negligible compared to the scattering from PEO-b-PNIPAM-b-PAA aggregates then from the SLS data treatment, $\frac{K_{pol}c_{pol}}{R(q=0,c)} = \frac{1}{M_w^{app}}$ an apparent molecular weight is obtained. This needs to be rescaled if we use polymer's parameters i.e. $K_{pol} = \frac{4\pi^2 n_0^2}{N_A \lambda^4}(\partial n/\partial c)_{pol}^2$ and c_{pol}. For $(\partial n/\partial c)_{pol}$ we use a weight average i.e. $(\partial n/\partial c)_{pol} = 0.07 \cdot (\partial n/\partial c)_{PEO} + 0.68 \cdot (\partial n/\partial c)_{PNIPAM} + 0.25 \cdot (\partial n/\partial c)_{PAA}$. For the additional mass percentage w due to lysozyme on one aggregate leads to a complex's molecular weight $M_w^{comp} = (1+w) \cdot M_w^{agg}$, where M_w^{agg} is the molecular mass of the aggregates before complexation. The concentration of the complexed particles is $(1+w) \cdot c_{pol}$ and their refractive index increment is $(\partial n/\partial c)_{comp} = \frac{1}{1+w}(\partial n/\partial c)_{pol} + \frac{w}{1+w}(\partial n/\partial c)_{lyso}$. From the equation $M_w^{app} \cdot K_{pol} \cdot c_{pol} = M_w^{comp} \cdot K_{comp} \cdot c_{comp}$ the mass percentage w is obtained (equation 3).

$$w = \left(\sqrt{\frac{M_w^{app}}{M_w^{mic}}} - 1\right) \cdot \frac{(\partial n/\partial c)_{pol}}{(\partial n/\partial c)_{lys}} \qquad (3)$$

From w the number of lysozyme globules per aggregate N_{glob} is calculated using the molecular weight of lysozyme.

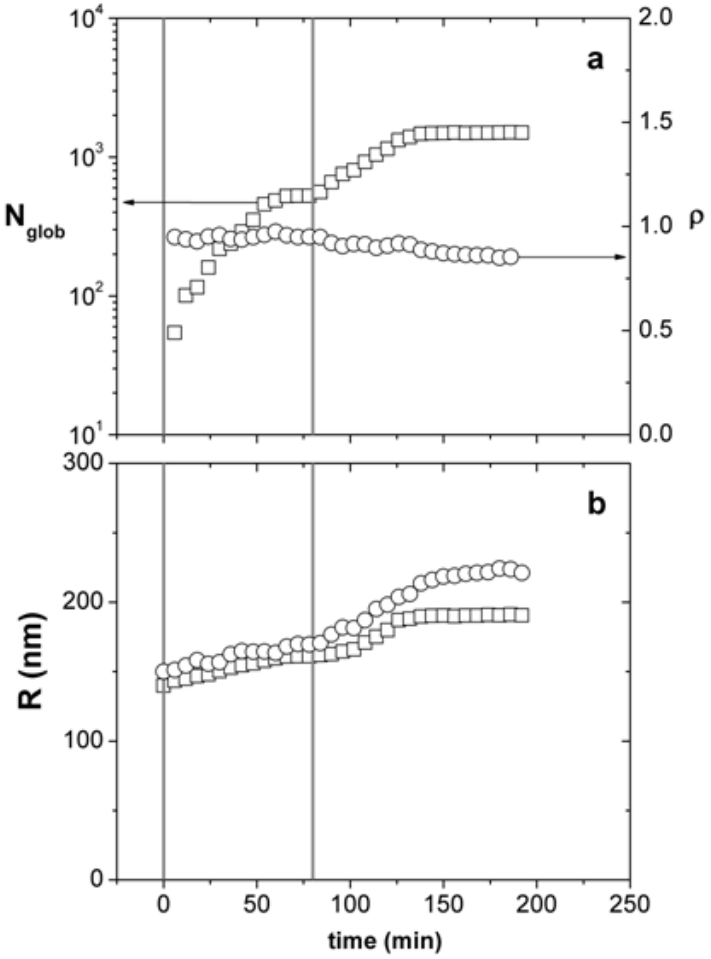

Figure 3: Number of lysozyme globules per micelle (squares) and characteristic ratio (circles) (a) and gyration (squares) and hydrodynamic radius (circles) (b) for PEO-b-PNIPAM-b-PAA (0.1mg/ml, pH 7 and 0.01M NaCl) during complexation with lysozyme (0.025mg/ml, pH 7 and 0.01M NaCl). The experiment is run at 25 ^{o}C.

In figure 3 the vertical line on the left indicates the instant when the two components i.e. PEO-b-PNIPAM-b-PAA solution is mixed with the lysozyme solution. The LS experiment follows the evolving parameters of the system during complexation at 25 ^{o}C. For about 80 minutes (right vertical line of figure 3) the radii increase weakly (figure 3a) while their ratio is fairly constant. At this time interval the number of

globules per aggregate is increasing strongly (roughly exponentially) until about 50 minutes and reaches a (local) plateau between 50 and 80 minutes (right vertical line in figure 3). The weak increase in radii and the stability of their ratio shows that the aggregates do not change their geometry significantly during complexation. The increase in molecular weight (which is translated into N_{glob}) without significant geometry change, points that lysozyme globules enter the aggregates, complex probably mostly with the oppositely charged PAA chains, following the morphology of the PEO-b-PNIPAM-b-PAA and imposing also a mild swelling upon the aggregates. This process appears to reach equilibrium between 50 and 80 minutes.

From 80 minutes to the end of the experiment, another process occurs (figure 3). Initially N_{glob} increases exponentially (up to ~150 minutes) and reaches a plateau afterwards. Similarly the radii increase and reach a plateau at roughly the same time. The final values of the radii produce a lower value of ρ due to stronger increase of R_h than R_g. This value of $\rho \approx 0.85$ indicates a trend of the clusters to form a more compact spherical structure. At the point of the vertical line at 80 minutes the total amount of lysozyme that is complexed on aggregates is approximately equal to the amount of lysozyme dissolved in solution. Any N_{glob} higher than this value (~500 globules/aggregate) is not feasible and hence values $N_{glob} > 500$ are apparently caused by clustering between aggregates that increase the total molecular weight. In conclusion, at 80 minutes the loading of single aggregates by lysozyme has reached its end-point and afterwards a second process of inter-aggregate clustering mediated by lysozyme takes place.

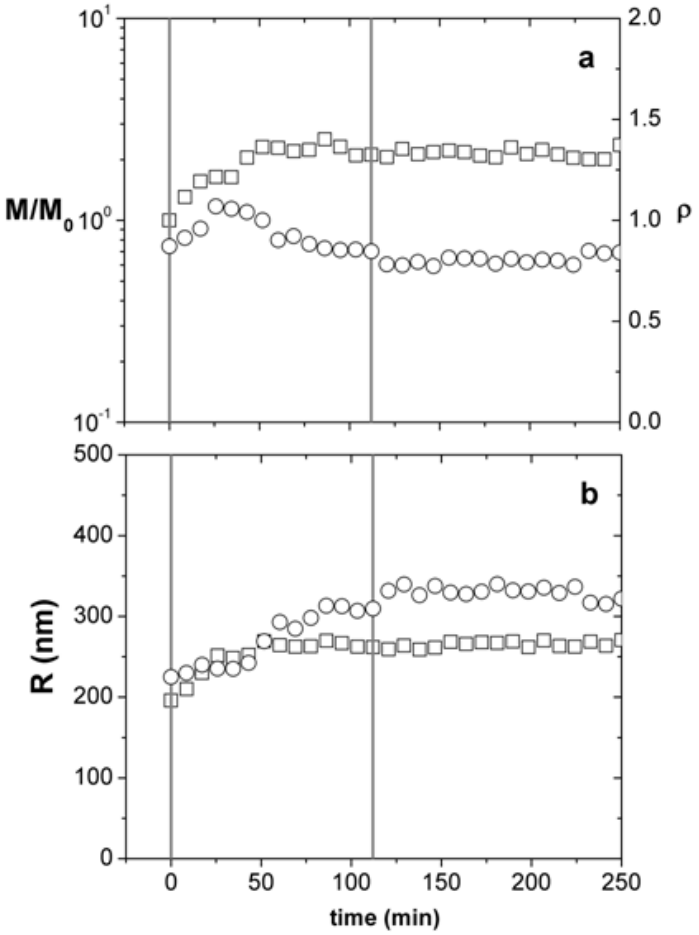

Figure 4: Relative molecular weight (squares) and characteristic ratio (circles) (a) and radius of gyration (squares) and hydrodynamic radius (circles) (b) for PEO-b-PNIPAM-b-PAA/lysozyme complexes (0.1/0.025mg/ml, pH 7 and 0.01M NaCl). The vertical lines indicate the jump from 30 to 35 °C (left) and from 35 to 30 °C (right).

In figure 4 the kinetics of the formed PnBA-b-PNIPAM-b-PAA / lysozyme complexes through the two temperature jumps is shown. Upon the increase in temperature the molecular weight of the clusters increases for 70-80 minutes before it reaches equilibrium. The ratio M/M_0 is the ratio of the apparent molecular weight (as obtained by the Guinier approximation) at a certain time over the molecular weight of the clusters at the first temperature jump (time=0). The increased hydrophobicity of the PNIPAM blocks cause further clustering of the complexes increasing the

molecular weight by 2-3 times. At the same time the radii increase mildly while R_g reaches a plateau value sooner than R_h. This latter effect results to a final decrease in ρ towards a compact spherical conformation. After reducing the temperature below PNIPAM's LCST the complexes are virtually unaltered. Probably the bonds created while PNIPAM is in its globule state and caused the partial irreversibility in the case of the pure polymer aggregates (with no added lysozyme) are now enhanced by the presence of lysozyme which also contains hydrophobic domains (ref). This way the combination of lysozyme and PEO-b-PNIPAM-b-PAA aggregates create a hybrid nanostructure that is irreversibly transformed to a compact structure upon the increasing-temperature jump.

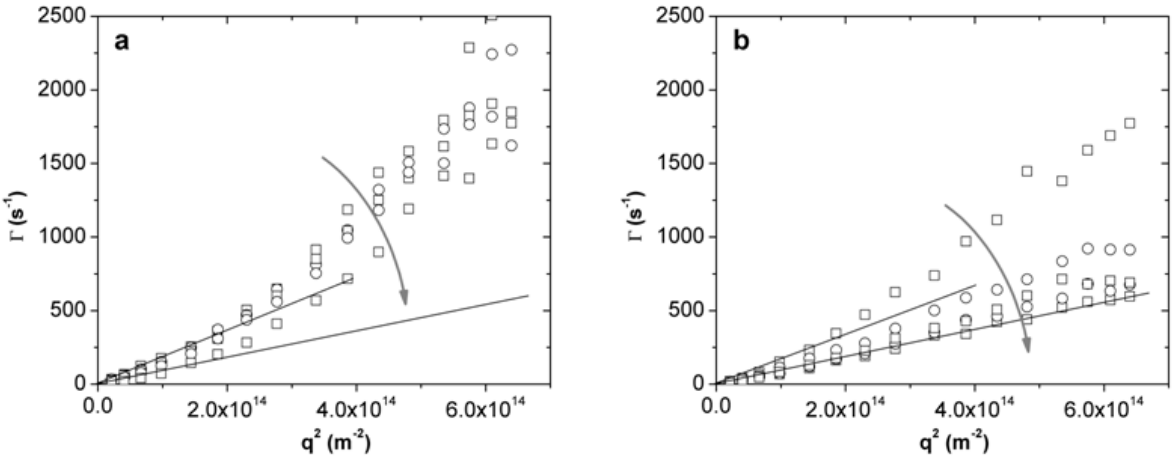

Figure 5: DLS characteristic main relaxation rates from (a) PEO-b-PNIPAM-b-PAA/lysozyme complexation and (b) PEO-b-PNIPAM-b-PAA/lysozyme complexes from successive runs (equal time intervals) over the whole experiments described in figures 3 and 4. The straight lines are fits at the linear part of the data sets.

At this point it is worth looking at the details of the $\Gamma(q)$ vs q^2 of this study. For the case of temperature jumps (figures 1b and 5b) the plots are initially highly non-linear

and eventually linear after some time well within the increasing-temperature jump. After this point and even after the decrease in temperature back to 30 °C the plots remain linear for both PEO-b-PNIPAM-b-PAA aggregates (data not shown) and PEO-b-PNIPAM-b-PAA/lysozyme complexes (figure 5b). In figure 6 we observe that for all the experiments performed in this study the distributions of relaxation rates is fairly narrow and obviously dominated by a single species. The distribution functions equally spaced in time of the complete experiments are shown in figure 6. No systematic change with time is observed. Hence we can assume that the non-linearity of the $\Gamma(q)$ vs q^2 plots is due to some internal dynamic relaxations of the aggregates[30]. Upon increase of temperature and the coil-to-globule transition of PNIPAM the stronger binding between chains (and/or chain-lysozyme in the case of complexes) freeze and the plots become linear as in the case of solid, internally rigid bodies. This freezing remains after the return of temperature below LCST which is in accordance to the partial irreversibility of the aggregates and the total irreversibility of the complexes. In the case of complexation of PEO-b-PNIPAM-b-PAA with lysozyme below LCST (figure 5a) the non-linearity of the plots is observed through the whole experiment showing that lysozyme allows internal dynamical relaxations during its binding.

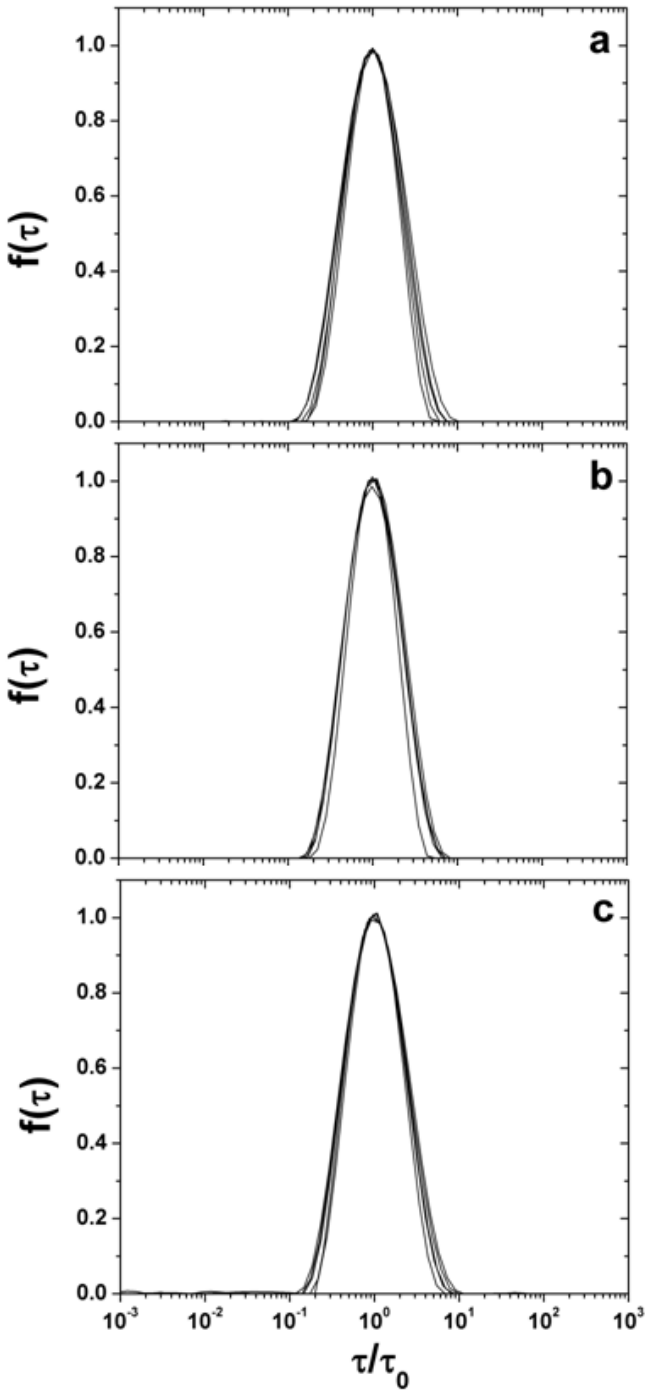

Figure 6: Relaxation time distributions (CONTIN) as a function of time (normalized by the main relaxation time) for the three experiments: (a) Temperature jumps of PEO-b-PNIPAM-b-PAA aggregates, (b) Complexation of PEO-b-PNIPAM-b-PAA aggregates with lysozyme and (c) Temperature jumps of PEO-b-PNIPAM-b-PAA / lysozyme aggregates.

CONCLUSIONS

Multi-Angle Laser Light Scattering was used to characterize thermoresponsive and complexation in PEO-b-PNIPAM-b-PAA / lysozyme aqueous solutions. At room temperature PEO-b-PNIPAM-b-PAA form aggregates that upon increase in temperature from 30 to 35 °C initially shrink and finally create inter-aggregate clusters. The initial microgel/fractal aggregate structure changes to core-shell-like geometry. The kinetics of complexation of lysozyme with the aggregates (formed at room temperature) is initially dominated by the loading of protein globules on aggregates and finally by protein-mediated inter-aggregate clustering. This clustering is further enhanced upon increase of temperature. Interestingly, there is evidence that internal dynamics of PEO-b-PNIPAM-b-PAA aggregates and PEO-b-PNIPAM-b-PAA / lysozyme complexes "freeze" irreversibly during the increasing-temperature-jump. This study proves the importance of the kinetics studies in these systems and creates ground for further analytical experiments as a function of polymer concentration, target temperatures, salt content and pH in order to reveal the responsiveness of the self-assembled nanosystems.

ACKNOWLEDGEMENTS:

Authors acknowledge financial support of the work by the NANOMACRO 1129 project which is implemented in the framework of the Operational Program "Education and Life-long Learning" (Action "ARISTEIA I") and it is co-funded by the European Union (European Social Fund) and by national funds. Light scattering

was conducted at the Center for Nanophase Materials Sciences, which is a DOE Office of Science User Facility.

REFERENCES

1. Stuart, M. A. C.; Huck, W. T. S.; Genzer, J.; Muller, M.; Ober, C.; Stamm, M.; Sukhorukov, G. B.; Szleifer, I.; Tsukruk, V. V.; Urban, M.; Winnik, F.; Zauscher, S.; Luzinov, I.; Minko, S. *Nat Mater* **2010,** 9, (2), 101-113.

2. Torchilin, V. P. *Journal of Controlled Release* **2001,** 73, (2–3), 137-172.

3. Ballauff, M. *Prog. Polym. Sci.* **2007,** 32, 1135–1151.

4. Kabanov, A.; Vinogradov, S., Nanogels as Pharmaceutical Carriers. In *Multifunctional Pharmaceutical Nanocarriers*, Torchilin, V., Ed. Springer New York: 2008; Vol. 4, pp 67-80.

5. Ryu, J.-H.; Chacko, R. T.; Jiwpanich, S.; Bickerton, S.; Babu, R. P.; Thayumanavan, S. *Journal of the American Chemical Society* **2010,** 132, (48), 17227-17235.

6. Klouda, L.; Mikos, A. G. *European Journal of Pharmaceutics and Biopharmaceutics* **2008,** 68, (1), 34-45.

7. Hoare, T. R.; Kohane, D. S. *Polymer* **2008,** 49, (8), 1993-2007.

8. Chu, B., *Laser Light Scattering*. 2 ed.; Academic Press: New York, 1991.

9. Berne, B. J.; Pecora, R., *Dynamic Light Scattering, With Applications to Chemistry, Biology, and Physics*. Dover: Toronto, 2000.

10. Feigin, L. A.; Svergun, D. I., *Structure Analysis by Small-Angle X-Ray and Neutron Scattering*. Plenum Press, New York and London: 1987.

11. Sorensen, C. M. *Aerosol Sci. Technol.* **2001,** 35, (2), 648-687.

12. Chu, B.; Wang, Z.; Yu, J. *Macromolecules* **1991,** 24, (26), 6832-6838.

13. Devanand, K.; Selser, J. C. *Macromolecules* **1991,** 24, (22), 5943-5947.

14. Kubota, K.; Hamano, K.; Kuwahara, N.; Fujishige, S.; Ando, I. *Polym J* **1990,** 22, (12), 1051-1057.

15. Colombani, O.; Ruppel, M.; Burkhardt, M.; Drechsler, M.; Schumacher, M.; Gradzielski, M.; Schweins, R.; Müller, A. H. E. *Macromolecules* **2007,** 40, (12), 4351-4362.

16. Papagiannopoulos, A.; Zhao, J.; Zhang, G.; Pispas, S.; Radulescu, A. *Polymer* **2013,** 54, (23), 6373-6380.

17. Papagiannopoulos, A.; Zhao, J.; Zhang, G.; Pispas, S.; Radulescu, A. *European Polymer Journal* **2014,** 56, (0), 59-68.

18. Khutoryanskiy, V. V.; Staikos, G., *Hydrogen-Bonded Interpolymer Complexes: Formation, Structure and Applications* World Scientific: 2009.

19. Papagiannopoulos, A.; Karayianni, M.; Mountrichas, G.; Pispas, S.; Radulescu, A. *Polymer* **2015**, (0).

20. Wu, C.; Wang, X. *Physical Review Letters* **1998,** 80, (18), 4092-4094.

21. Adelsberger, J.; Grillo, I.; Kulkarni, A.; Sharp, M.; Bivigou-Koumba, A. M.; Laschewsky, A.; Muller-Buschbaum, P.; Papadakis, C. M. *Soft Matter* **2013,** 9, (5), 1685-1699.

22. Adelsberger, J.; Metwalli, E.; Diethert, A.; Grillo, I.; Bivigou-Koumba, A. M.; Laschewsky, A.; Müller-Buschbaum, P.; Papadakis, C. M. *Macromolecular Rapid Communications* **2012,** 33, (3), 254-259.

23. Schmitz, K. S.; Wang, B.; Kokufuta, E. *Macromolecules* **2001,** 34, (23), 8370-8377.

24. Van Saarloos, W. *Physica A* **1987,** 147, 280-296.

25. Hirzinger, B.; Helmstedt, M.; Stejskal, J. *Polymer* **2000,** 41, (8), 2883-2891.

26. Müller, A.; Burchard, W. *Colloid Polym Sci* **1995,** 273, (9), 866-875.

27. Boyko, V.; Pich, A.; Lu, Y.; Richter, S.; Arndt, K.-F.; Adler, H.-J. P. *Polymer* **2003,** 44, (26), 7821-7827.

28. Hirokawa, Y.; Tanaka, T. *The Journal of Chemical Physics* **1984,** 81, (12), 6379-6380.

29. Azegami, S.; Tsuboi, A.; Izumi, T.; Hirata, M.; Dubin, P. L.; Wang, B.; Kokufuta, E. *Langmuir* **1999,** 15, (4), 940-947.

30. Galinsky, G.; Burchard, W. *Macromolecules* **1997,** 30, (22), 6966-6973.